Supporting Information for:

The copper active site in CBM33 polysaccharide oxygenases

Glyn R. Hemsworth, Edward J. Taylor, Robbert Q. Kim, Rebecca C. Gregory, Sally J. Lewis, Johan P. Turkenburg, Alison Parkin, Gideon J. Davies* and Paul H. Walton*

Department of Chemistry, University of York, Heslington, York YO10 5DD, U.K.

Table S1. Data Processing and Refinement Statistics for BaCBM33 Structures.

Data Processing Dataset		*Apo*		Cu-Bound		Cu-bound/Ascorbate Soak	
Space Group		$P2_12_12_1$		$P2_1$		$P2_12_12_1$	
Cell Dimensions							
a (Å)	α (°)	66.5	90.0	34.8	90.0	66.4	90.0
b (Å)	β (°)	77.7	90.0	73.5	100.3	77.2	90.0
c (Å)	γ (°)	72.5	90.0	75.8	90.0	73.9	90.0
No. of molecules in asymmetric unit		2		2		2	
Resolution (Å)		49.00-1.80 (1.90-1.80)		19.93-1.90 (2.00-1.90)		41.60-1.70 (1.79-1.70)	
Beamline		Diamond I04-1		Diamond I04-1		Diamond I03	
Wavelength (Å)		0.917		0.917		0.976	
Observed/unique reflections		283,432/35,052		108,335/29,332		274,822/42,480	
R_{merge} (%)		11.0 (73.3)		12.0 (47.7)		14.3 (81.7)	
R_{pim} (%)		4.1 (26.8)		7.3 (29.2)		6.1 (34.5)	
Multiplicity		8.1 (8.3)		3.7 (3.7)		6.2 (6.4)	
Completeness (%)		98.3 (95.4)		98.8 (99.1)		99.9 (99.9)	
Mean(I/σ(I))		10.9 (2.7)		9.3 (2.7)		8.2 (2.6)	
Refinement Statistics							
Number of reflections (working/free sets)		33,214/1,789		27,833/1,481		40,263/2,150	
Number of atoms		3,065		3,003		3,103	
Average B-factors for all atoms		23.1 $Å^2$		16.1 $Å^2$		16.9 $Å^2$	
R_{work}/R_{free}		0.234/0.281		0.215/0.270		0.209/0.248	
RMS deviation from ideality:							
Bond lengths		0.015 Å		0.012 Å		0.015 Å	
Bond angles		1.55°		1.54°		1.54°	
Chiral Volume		0.10 $Å^3$		0.09 $Å^3$		0.11 $Å^3$	
ΔB factors of bonded atoms:							
overall		5.1 $Å^2$		5.4 $Å^2$		4.1 $Å^2$	
mainchain		3.3 $Å^2$		4.2 $Å^2$		2.4 $Å^2$	
sidechain		7.3 $Å^2$		6.8 $Å^2$		6.1 $Å^2$	

Ramachandran plot. Proportion of residues in (%):			
favored regions	98.2%	98.0%	98.3%
allowed regions	100.0%	100.0%	100.0%
disallowed regions	0.0%	0.0%	0.0%
PDB Identifier	2YOW	2YOX	2YOY

Statistics in parentheses represent data in the highest resolution shell.

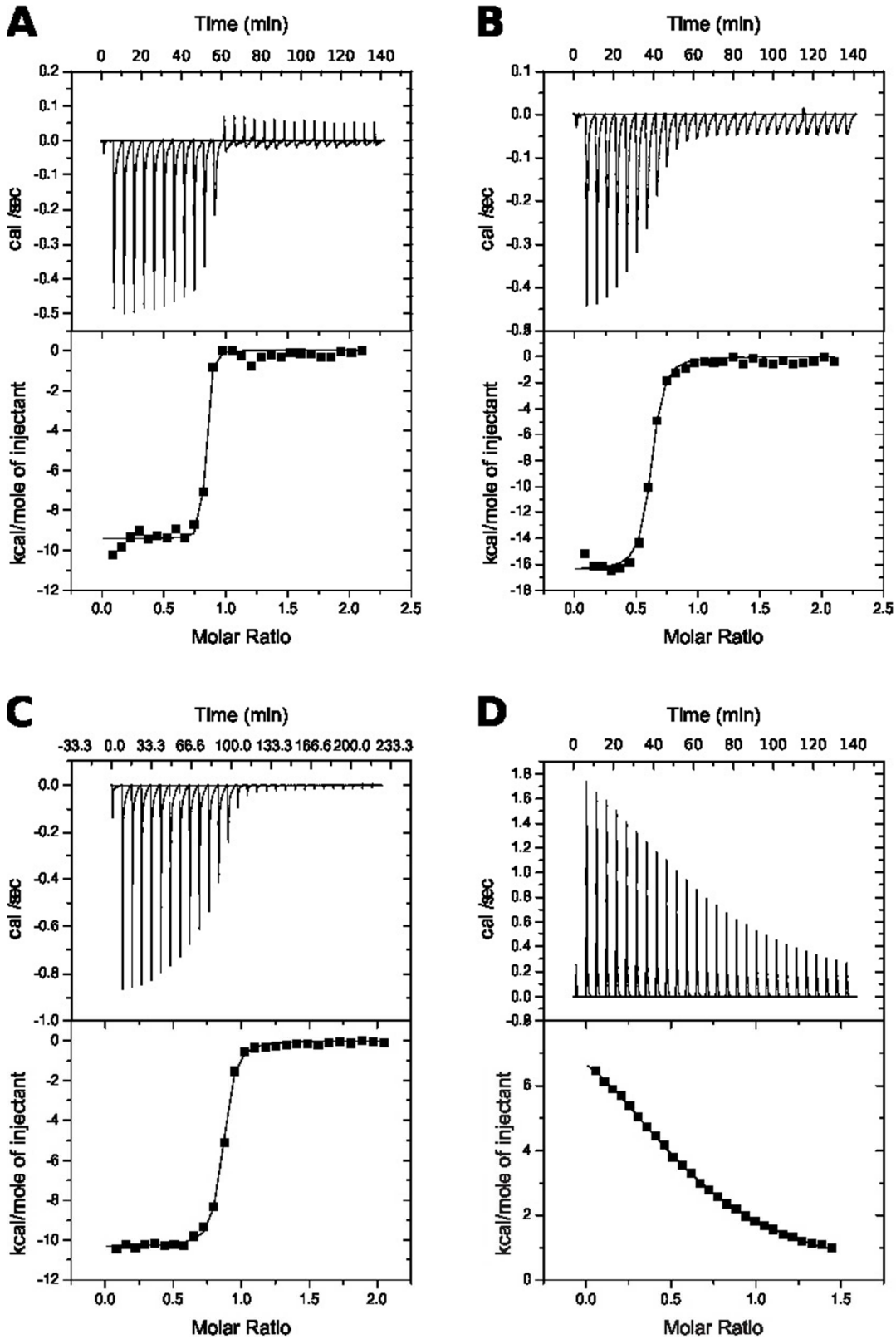

Figure S1. Isothermal Calorimetry showing (A) Cu binding at pH 5.0, (B) pH 6.0 (C) pH 7.0 and (D) Zn binding at pH 5.0 with a K_d of 37.5 μM .

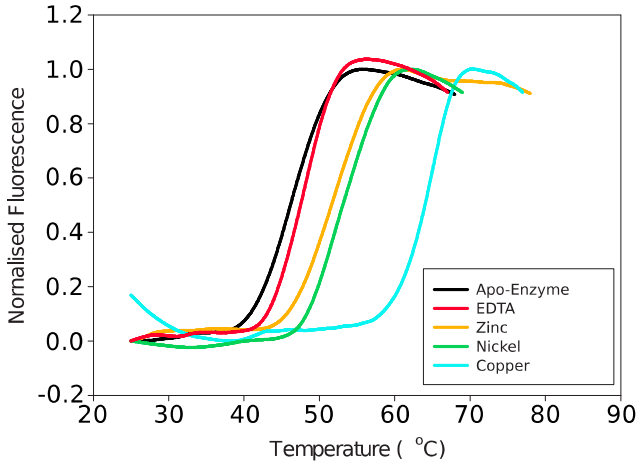

Figure S2. Melting curves for *Ba*CBM33 in the presence of EDTA and different metal ions. The fluorescence difference across the melting curve has been normalised for clarity due to significant fluorescence quenching in the presence of copper. The melting temperatures (T_m) determined by curve fitting to these data were *apo*-enzyme = 46°C, EDTA = 48°C, zinc = 52°C, nickel = 53°C, and copper = 65°C. Significant increases in thermostability were observed in response to all three metals but copper showed the largest increase suggesting the tightest binding to the protein.

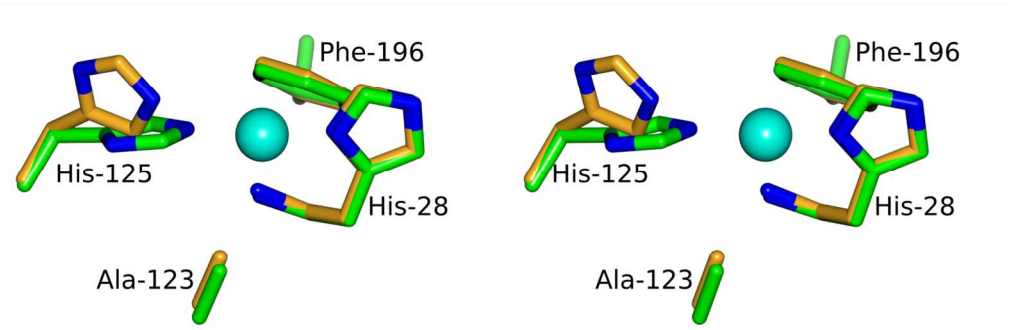

Figure S3. The arrangement of the active site residues in the copper complex (green) and *Apo* (orange) structures shown in stereo. All side chains occupy identical positions apart from His-125 which is rotated away in the absence of copper. Figure prepared with CCP4MG [1].

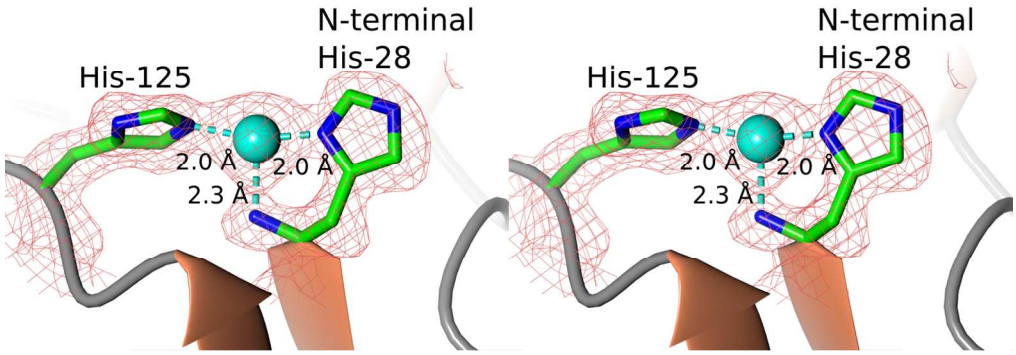

Figure S4. The electron density in the BaCBM33 Cu complex active site contoured at 1σ in divergent stereo. The N-terminal histidine brace coordination around the copper ion is shown.

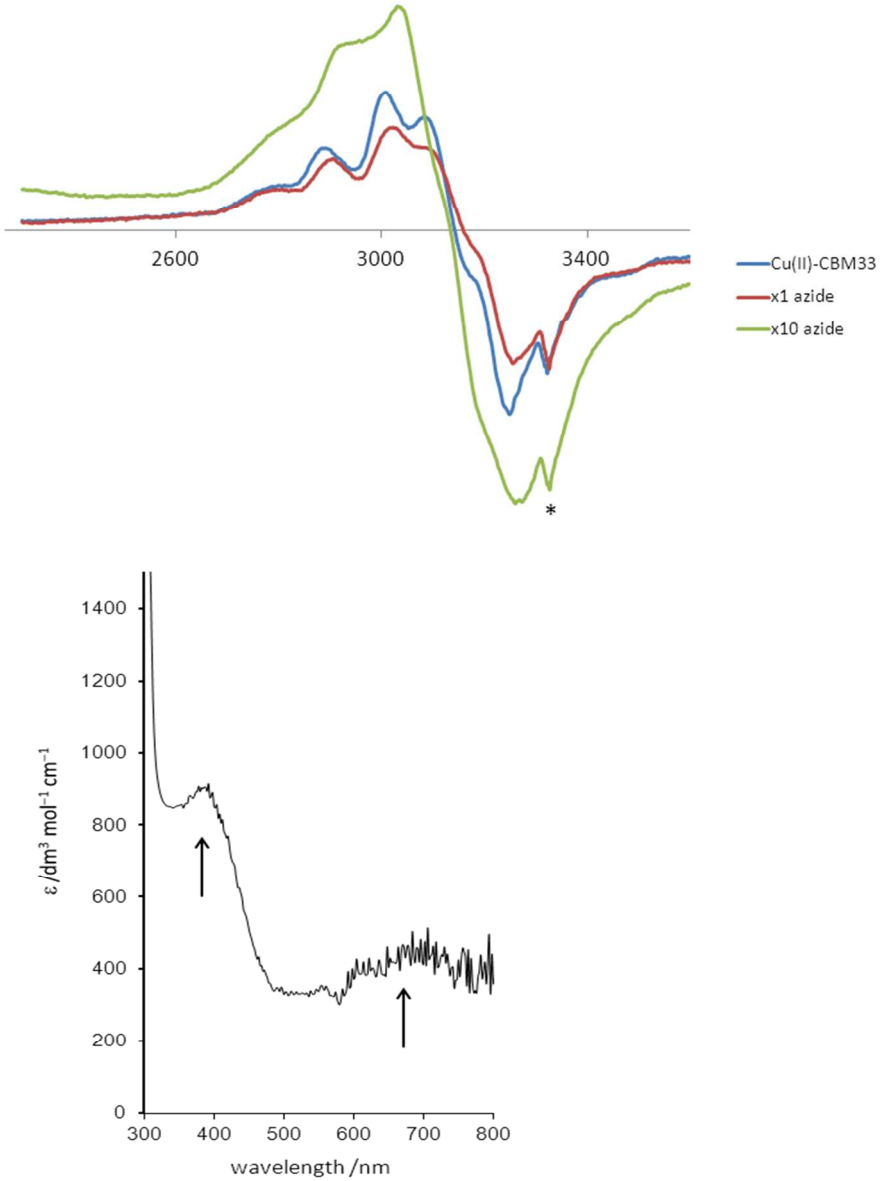

Figure S5. Changes upon addition of stoichiometric azide and excess azide to CuBaCBM33 left) in X-band (9 GHz) EPR spectrum of 0.2 mM solution of Cu(II)BaCBM33 at pH 5 (blue spectrum) on addition of stoichiometric sodium azide (red spectrum). * = marker, and right) UV/vis spectrum showing growth of bands with excess (x10) azide.

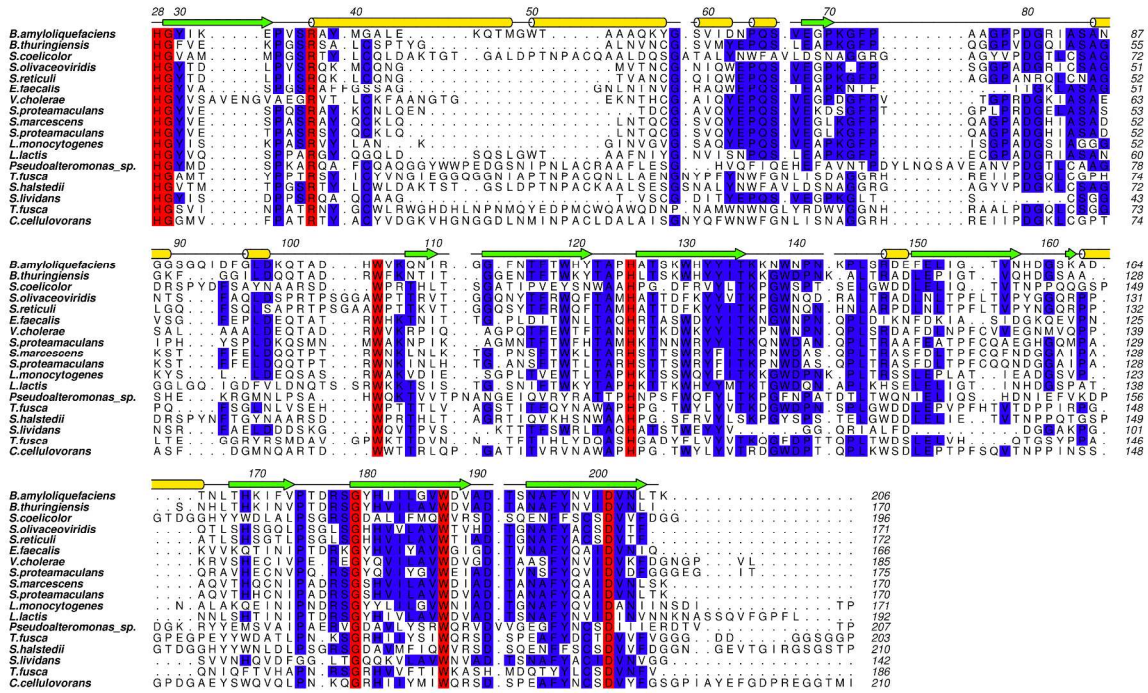

Figure S6. Amino acid sequence alignment of *Ba*CBM33 with a range of selected CBM33s. Red = 100% conservation, blue = 50-99% conservation. L2 alpha-helical loop region is between residues 37 and 66.

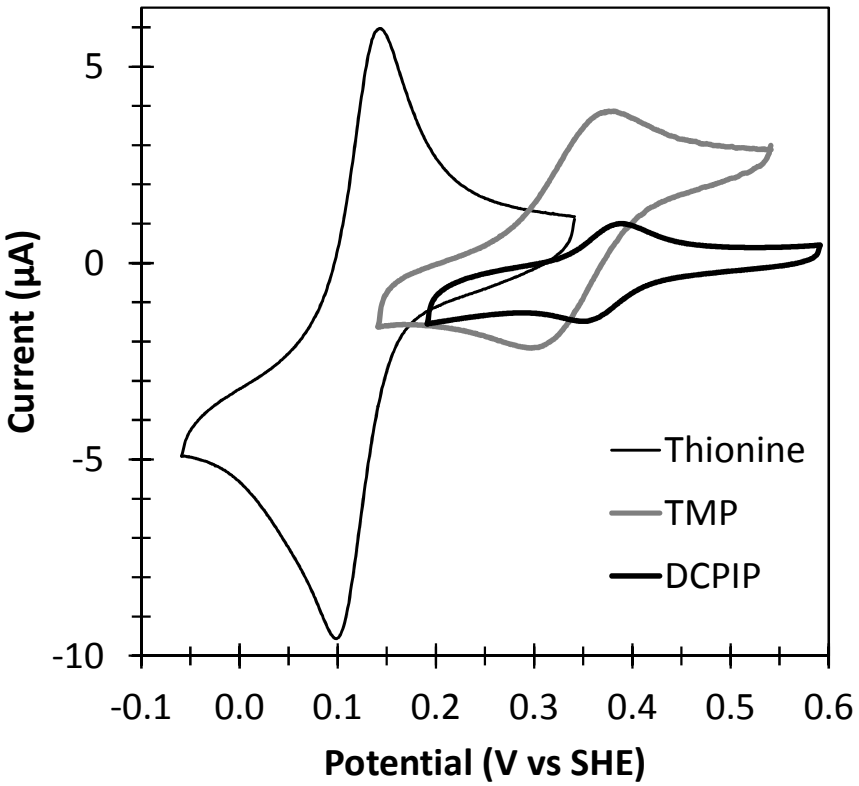

S7: Cyclic voltammograms to determine the reduction potentials of different redox indicators in 100 mM sodium acetate buffer, pH 5. Experiments were conducted at 20 °C using 1 mM solutions of each compound. The scans were measured at 50 mVs^{-1} under an atmosphere of Ar.

A three-electrode set up was used to determine the reduction potential of the redox indicators thionine, TMP and DCPIP in 100 mM sodium acetate buffer, pH 5. A stationary Pt disc working electrode (BASi), a Pt wire counter electrode and a saturated calomel reference electrode (SLS) were all placed into an all-glass electrochemical cell. Cyclic voltammograms (50 mVs^{-1}) were then measured for 1 mM solutions of each of the redox compounds under a flow of Ar. A correction factor of $E_{SHE} = E_{SCE} + 0.241$ V was used to convert the potentials from Volts versus saturated calomel reference electrode (SCE) to Volts versus standard hydrogen electrode (SHE). The resultant scans are shown in Figure S7. The anodic and cathodic peak potentials, as determined by the electrochemical software (Epsilon BASi), were averaged to give the midpoint reduction potentials, summarised in Table S1. Cu(II)*Ba*CBM33 gave oxidation of dyes with midpoint redox potentials ≤330 mV but not ≥ 370 mV at pH 5 vs SHE, which—after correction for an estimated 9:1 reduced:oxidised dye ratio with the Nernst equation (56 mV)—gives a redox range of ca 275 to 370 mV.

Redox dye compound	**Reduction potential in pH 5 acetate buffer (V *vs* SHE)**
Thionine	+0.12
TMP	+0.33
DCPIP	+0.37

Table S2. Reduction potentials determined from the data in Figure S7

References

(1) McNicholas, S.; Potterton, E.; Wilson, K. S.; Noble, M. E. M. *Acta Crystallographica Section D* **2011**, *67*, 386.